

Improved DTC Control Strategy of B12 Inverter Fed BLDC Motor Drives Considering Commutation Torque Dips

Rabiaa Mars*, Badii Bouzidi, Bassem El Badsii, Abderrazak Yangui

University of Sfax, Electrical Department, Sfax Engineering National School, P.O. Box 1173, 3038 Sfax, Tunisia

ARTICLE INFO

Article history:

Received: 10 July, 2018

Accepted: 09 October, 2018

Online: 24 October, 2018

Keywords:

Brushless DC motor

Commutation torque dips

Direct torque control scheme

Current slope

Simulation results

ABSTRACT

In most industrial high-power applications, the brushless DC (BLDC) motor is connected to multi-level inverters specially the three-level NPC inverters (B12). Torque ripple is a critical issue in BLDC motor drives. Accordingly, minimizing the ripple produced in the torque is necessary to enhance the BLDC motor drive performances. This paper aims to develop two direct torque control (DTC) schemes. To evaluate the proposed strategies performances, three DTC schemes, namely DTC-1, DTC-2, and DTC-3, are treated. The DTC-1 scheme is inspired from the Takahashi's strategy proposed in induction motor drives. This scheme is penalized by the high torque dips. In view of that, the DTC-2 is proposed to address the DTC-1 limitations. Simulation evaluation proves that difference between the slopes of the incoming and outgoing phases currents procreates commutation torque dips penalizing the DTC-2 scheme. This difference is more serious at high speed. To overcome the DTC-2 strategy drawbacks, a DTC-3 scheme, based on the compensation of this difference, is proposed. Taking into account the increase of this difference with the increase of the rotation speed, the vector selection table design of this strategy is synthesized to minimize the torque ripple as far as possible.

1 Introduction

The use of three-level NPC (B12) inverter in high-power applications increases due to their performances [1]-[2]. Indeed, compared to the two-level inverter, the B12 inverter offers the low output current distortion and operates with reduced dv/dt stress [3]-[4]-[5]-[6].

Due to its numerous advantages as its simple structure, low noise, good stability and high efficiency [7]-[8]-[9], BLDC motor is extensively used in numerous industrial applications. Conversely, the torque ripple is a critical issue in BLDC motor drives [10]-[11]-[12]. Accordingly, minimizing the ripple produced in the torque is necessary to enhance the performances of BLDC motor drive system [13]-[14].

The present paper proposes two DTC strategies dedicated to the BLDC motor fed by three-level (B12) inverter. It has been found that commutation torque ripple is a main problem penalizing the first proposed strategy. This commutation phenomenon af-

fects the industrial applications needing high performance [15]-[16]. It leads to a deteriorating efficiency of the BLCD motor. Hence, the second proposed strategy aims to address these drawbacks.

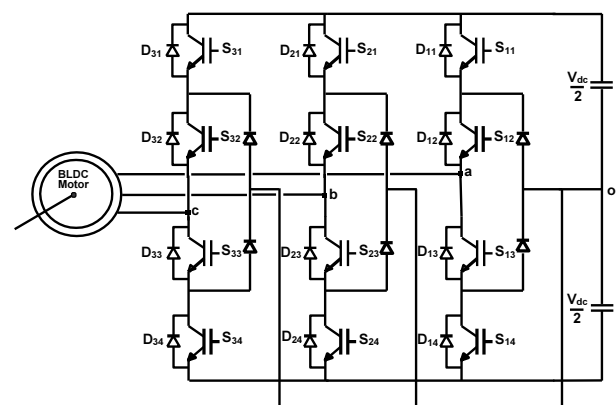


Figure 1: B12 inverter with BLDC motor connected.

*Rabiaa Mars, Sfax Engineering National School, marsrabiaa@yahoo.com

2 Analysis of the BLDC motor operation

The B12 inverter is connected with BLDC motor as illustrated in Figure.1

The rectangularly shaped currents(i_a, i_b, i_c) fed BLDC motor are synchronized with the trapezoidal back-EMFs(e_a, e_b, e_c) to accomplish a constant torque with reduced dips as shown in Figure.2.

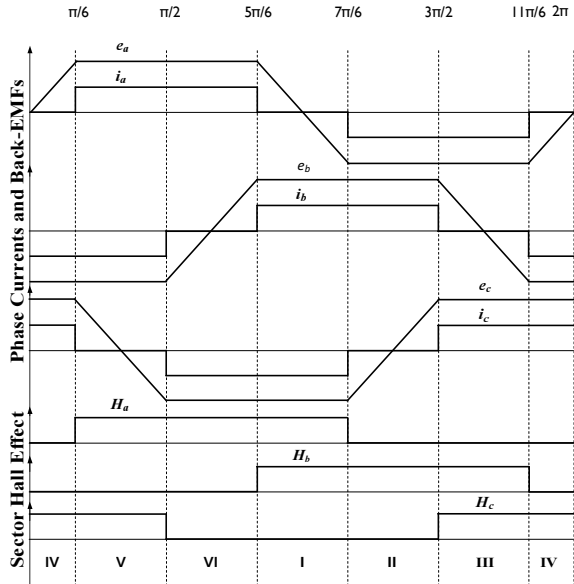


Figure 2: Back-EMFs, phase currents and the corresponding Hall-effect signals of BLDC motor .

The BLDC motor stator voltages (v_a, v_b, v_c) are given by:

$$\begin{cases} v_a = Ri_a + (L-M)\frac{di_a}{dt} + e_a; \\ v_b = Ri_b + (L-M)\frac{di_b}{dt} + e_b; \\ v_c = Ri_c + (L-M)\frac{di_c}{dt} + e_c. \end{cases} \quad (1)$$

Where:

- Resistance: $R (\Omega)$,
- Self inductance: $L(H)$,
- Mutual inductance: $M(H)$.

The produced torque T_{em} is given as:

$$T_{em} = \frac{e_a i_a + e_b i_b + e_c i_c}{\Omega} \quad (2)$$

Where Ω represents the angular speed.

Under two-phase conduction mode, the B12 inverter engenders six Half voltage vectors (V_1 to V_6) and six Intermediate Voltage Vectors (V_7 to V_{12}).

Under three-phase conduction mode, the B12 inverter generates three null vectors (U_{01} to U_{03}), six

Intermediate voltage vectors (U_1 to U_6) and six Full Voltage Vectors (U_7 to U_{12}).

Tables.1 and 2 provide the switch state combinations.

Table 1: Active voltage vectors under the two-phase conduction mode.

| ($S_a S_b S_c$) | V_α | V_β | Vectors |
|------------------------------|-------------------------------|------------------------------|----------|
| Half Voltage Vectors | | | |
| (1100 0000 0000) | $\frac{1}{\sqrt{6}} V_{dc}$ | 0 | V_1 |
| (0000 0000 0011) | $\frac{1}{\sqrt{24}} V_{dc}$ | $\frac{1}{\sqrt{8}} U_c$ | V_2 |
| (0000 1100 0000) | $-\frac{1}{\sqrt{24}} V_{dc}$ | $\frac{1}{\sqrt{8}} U_c$ | V_3 |
| (0011 0000 0000) | $-\frac{1}{\sqrt{6}} V_{dc}$ | 0 | V_4 |
| (0000 0000 1100) | $-\frac{1}{\sqrt{24}} V_{dc}$ | $-\frac{1}{\sqrt{8}} U_c$ | V_5 |
| (0000 0011 0000) | $\frac{1}{\sqrt{24}} V_{dc}$ | $-\frac{1}{\sqrt{8}} U_c$ | V_6 |
| Intermediate Voltage Vectors | | | |
| (1100 0000 0011) | $\sqrt{\frac{3}{8}} V_{dc}$ | $\frac{1}{\sqrt{8}} V_{dc}$ | V_7 |
| (0000 1100 0011) | 0 | $\frac{1}{\sqrt{2}} V_{dc}$ | V_8 |
| (0011 1100 0000) | $-\sqrt{\frac{3}{8}} V_{dc}$ | $\frac{1}{\sqrt{8}} V_{dc}$ | V_9 |
| (0011 0000 0011) | $-\sqrt{\frac{3}{8}} V_{dc}$ | $-\frac{1}{\sqrt{8}} V_{dc}$ | V_{10} |
| (0000 0011 1100) | 0 | $-\frac{1}{\sqrt{2}} V_{dc}$ | V_{11} |
| (1100 0011 0000) | $\sqrt{\frac{3}{8}} V_{dc}$ | $\frac{1}{\sqrt{8}} V_{dc}$ | V_{12} |

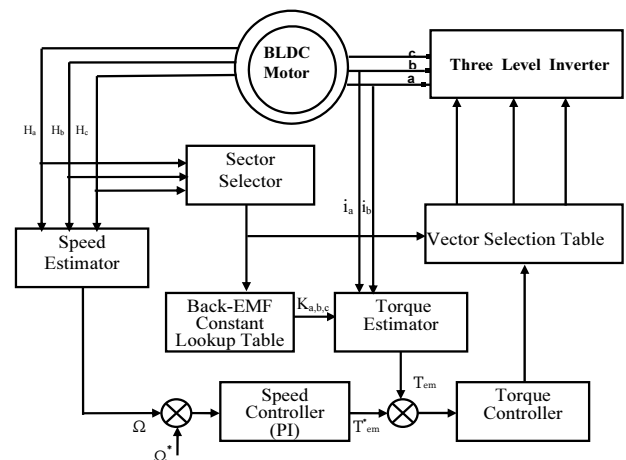


Figure 3: DTC scheme of the B12 inverter with BLDC motor connected.

3 Control strategies

3.1 DTC-1 strategy

The DTC-1 scheme is inspired from the one proposed by *Takahashi* in [17]. This strategy allows a direct control of the BLDC motor torque.

The DTC-1 scheme block diagram is illustrated in Figure.3. This diagram includes an hysteresis torque estimator which generates two outputs used to determine the vector selection table($c_\tau = +1$:torque increase, $c_\tau = -1$:torque decrease).

The switching table of this strategy is summarized in Table 3.

Table 3: The DTC-1 strategy vector selection table.

| c_τ | +1 | -1 |
|------------|-------------------------|-------------------------|
| Sector I | V_8 (0000 1100 0011) | V_{11} (000000111100) |
| Sector II | V_9 (001111000000) | V_{12} (110000110000) |
| Sector III | V_{10} (001100000011) | V_7 (110000000011) |
| Sector IV | V_{11} (000000111100) | V_8 (0000 1100 0011) |
| Sector V | V_{12} (110000110000) | V_9 (001111000000) |
| Sector VI | V_7 (110000000011) | V_{10} (001100000011) |

Table 2: Active voltage vectors under the three-phase conduction mode.

| $(S_a S_b S_c)$ | V_α | V_β | Vectors |
|------------------------------|-----------------------------|-----------------------------|----------|
| Intermediate Voltage Vectors | | | |
| (1100 0010 0011) | $\sqrt{\frac{3}{8}}V_{dc}$ | $\frac{1}{\sqrt{8}}V_{dc}$ | U_1 |
| (0100 1100 0011) | 0 | $\frac{1}{\sqrt{2}}V_{dc}$ | U_2 |
| (0011 1100 0010) | $-\sqrt{\frac{3}{8}}V_{dc}$ | $\frac{1}{\sqrt{8}}V_{dc}$ | U_3 |
| (0011 0100 0011) | $-\sqrt{\frac{3}{8}}V_{dc}$ | $-\frac{1}{\sqrt{8}}V_{dc}$ | U_4 |
| (0010 0011 1100) | 0 | $-\frac{1}{\sqrt{2}}V_{dc}$ | U_5 |
| (1100 0011 0100) | $\sqrt{\frac{3}{8}}V_{dc}$ | U_6 | |
| Full Voltage Vectors | | | |
| (1100 0011 0011) | $\sqrt{\frac{2}{3}}V_{dc}$ | 0 | U_7 |
| (1100 1100 0011) | $\frac{1}{\sqrt{6}}V_{dc}$ | $\frac{1}{\sqrt{2}}V_{dc}$ | U_8 |
| (0011 1100 0011) | $-\frac{1}{\sqrt{6}}V_{dc}$ | $\frac{1}{\sqrt{2}}V_{dc}$ | U_9 |
| (0011 1100 1100) | $-\sqrt{\frac{2}{3}}V_{dc}$ | 0 | U_{10} |
| (0011 0011 1100) | $-\frac{1}{\sqrt{6}}V_{dc}$ | $-\frac{1}{\sqrt{2}}V_{dc}$ | U_{11} |
| (1100 0011 1100) | $\frac{1}{\sqrt{6}}V_{dc}$ | $-\frac{1}{\sqrt{2}}V_{dc}$ | U_{12} |

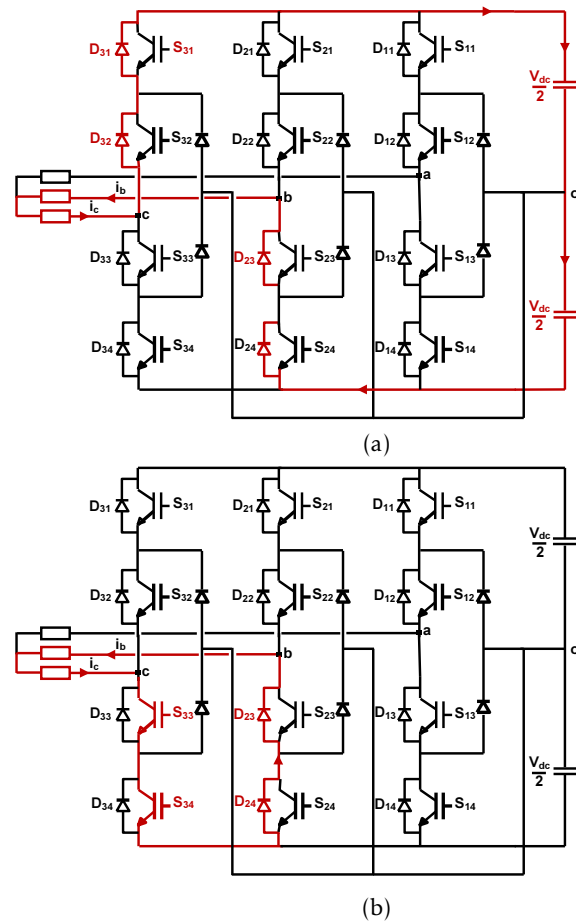


Figure 4: The current flowing during sector I in the case of a torque decrease under **Legend** (a): the DTC-1 scheme, (b): the proposed DTC-2 scheme.

3.2 DTC-2 strategy

It has been found that DTC-1 scheme is penalized by the high torque dips. In view of that, the DTC-2 is proposed to address the DTC-1 limitations. The control scheme of this strategy is similar to the one used in the DTC-1. The only difference is the control rules considered in the vector selection table.

Let's consider sector I, the vector selection table design of this scheme is synthesized as follows:

- To increase the torque, the DTC-2 scheme considers the same vectors applied in DTC-1,
- the vector V_2 achieves the torque decrease. As

illustrated in Figure. 4(b), the vector V_2 is defined by a freewheeling phase involving the two IGBTs S_{33} and S_{34} and the diodes D_{23} and D_{24} . Compared to DTC-2, the DTC-1 scheme considers the vector V_8 which characterized by a regenerative phase. During this phase, the currents i_c and i_b are forced to flow through the supply source V_{dc} and the diodes (D_{23}, D_{24}, D_{31} and D_{32}) as shown in Figure. 4(a). The currents slope observed under this phase has an absolute value higher than the one obtained under the freewheeling phase.

Consequently, the resulting DTC-2 strategy vector selection table is given in Table.4.

Table 4: The DTC-2 strategy vector selection table.

| c_τ | +1 | -1 |
|------------|------------------------|---------------------|
| Sector I | $V_8(000011000011)$ | $V_2(000000000011)$ |
| Sector II | $V_9(001111000000)$ | $V_3(000011000000)$ |
| Sector III | $V_{10}(001100000011)$ | $V_4(001100000000)$ |
| Sector IV | $V_{11}(000000111100)$ | $V_5(000000001100)$ |
| Sector V | $V_{12}(110000110000)$ | $V_6(000000110000)$ |
| Sector VI | $V_7(110000000011)$ | $V_1(110000000000)$ |

3.3 DTC-3 strategy

It has been found that DTC-2 scheme is penalized by the commutation torque ripple. As illustrated in Figure.5(a), the difference between the slopes of the incoming and outgoing phases currents generates commutation torque dips. In view of that, there is a necessity to make equal the rising time and the falling one of the phase currents as illustrated in Figure.5(b).

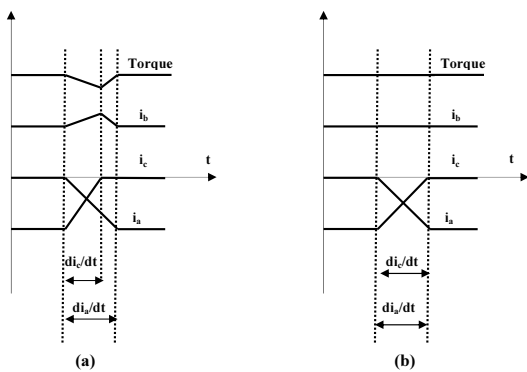


Figure 5: The behavior of the torque during commutation **Legend** (a): unequal slopes of the incoming and outgoing phases currents, (b): equal slopes of the incoming and outgoing phases currents.

The stator voltage equations of the BLDC motor are described by the equation (1). Neglecting the mutual inductance, v_a, v_b and v_c are given by the following system :

$$\begin{cases} v_a - e_a = Ri_a + L \frac{di_a}{dt} ; \\ v_b - e_b = Ri_b + L \frac{di_b}{dt} ; \\ v_c - e_c = Ri_c + L \frac{di_c}{dt} . \end{cases} \quad (3)$$

The Laplace Transform method can be used to solve this linear differential equations. Therefore the relation between the phase voltage and the phase current is dealt with using this method, and then the transfer function is similarly written as:

$$H(p) = \frac{v(p) - e(p)}{i(p)} = \frac{1}{Lp - R} \quad (4)$$

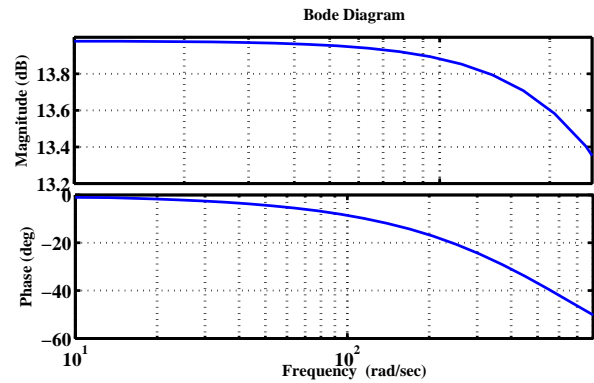


Figure 6: Approximated curve of the frequency response (bode-plot) of the BLDC motor.

Figure6 shows the approximated curve of the frequency response (bode-plot) based on equation (4). The plot displays the magnitude (in dB) and the phase (in degrees) of the system response as a function of frequency. Referring to this figure, the phase delay angle increases with the increase of the rotation speed. Moreover, this delay is more important at high speed. Consequently, the commutation torque dips is very serious at high speed.

To address the DTC-2 limitations, the third DTC scheme, noted DTC-3, is proposed . This strategy is based on the employ of a three-level torque controller. This controller generates 3 outputs as shown in Figure.7 :

- -1 corresponding to the torque decrease,
- +1 corresponding to the torque increase,
- +2 is activated when the torque drops during commutations from sector-to-sector .

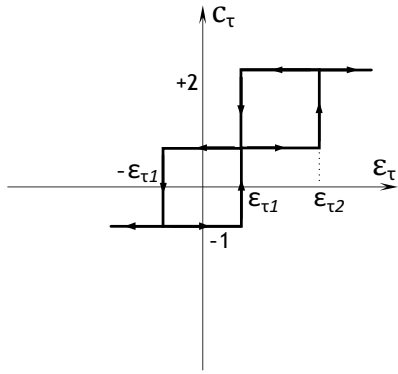


Figure 7: The three-level-torque controller characteristics.

Let’s consider sector I, the vector selection table design of this scheme is synthesized as follows:

- $c_τ = +1$ and $c_τ = -1$ are achieved by the same vectors used in DTC-2 scheme.
- The suppression of the commutation torque dips ($c_τ = +2$) is achieved by the application of the vectors corresponding to the three-phase conduction mode. To equalize $|di_a/dt|$ and $|di_c/dt|$, at the beginning of sector II, in the case of a reference speed $\Omega^* \leq \Omega_{limit}$, the current i_c is forced to flow through the IGBT S_{33} , the clamped diode and the supply source $\frac{V_{dc}}{2}$ instead of the uncontrollable diodes (D_{31} and D_{32}) as shown in Figures. 8(b) and 8(c). For a reference speed $\Omega > \Omega_{limit}$, the current i_c is forced to flow through the IGBTs (S_{33} , S_{34}) and the supply source V_{dc} instead of the uncontrollable diodes (D_{31} and D_{32}) as shown in Figures. 8(b) and 8(d).

Consequently, the resulting vector selection is given in Table.7.

4 Evaluation of the proposed DTC schemes effectiveness and performances

Simulation work has been accomplished to highlight the proposed strategies performances. Tables.5 and 6 gives the BLDC motor parameters and ratings.

Table 5: The ratings of BLDC motor

| | |
|----------------------|-------------------------|
| Current = 30A | DC voltage = 24V |
| Rated torque = 2.5Nm | PM flux-linkage = 14mWb |
| Power = 600W | Rated speed = 2500rpm |

Table 6: BLDC motor parameters

| | |
|-----------------|-----------------|
| $R = 0.2\Omega$ | $p = 3$ |
| $L = 0.3mH$ | $J = 4.1g.m^2$ |
| $R = 0.2\Omega$ | $f = 0.5mN.m.s$ |

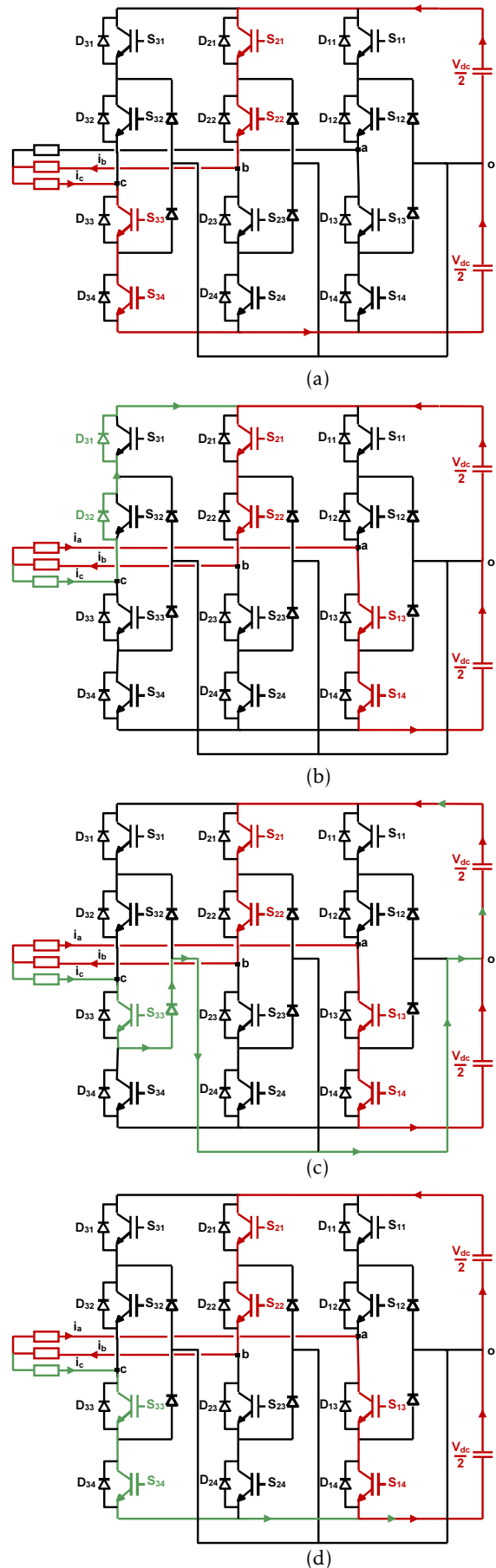
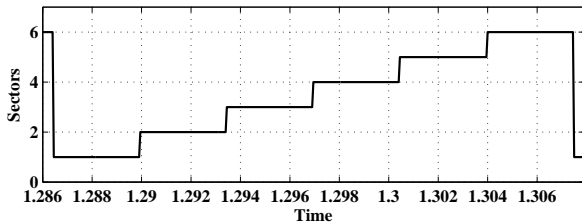


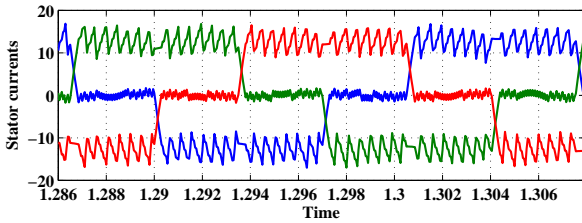
Figure 8: Current flowing during : Legend (a): sector I, (b): commutation under DTC-2 scheme, (c): commutation under DTC-3 scheme ($\Omega^* \leq \Omega_{limit}$) and (d): commutation under DTC-3 scheme ($\Omega^* > \Omega_{limit}$).

Table 7: The vector selection table of the DTC-3 strategy.

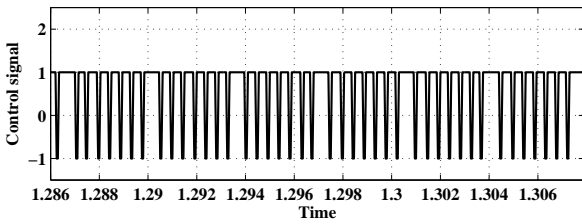
| c_τ | +1 | -1 | c_τ | +2 | |
|------------|------------------------|---------------------|------------------------|--------------------------------|-----------------------------|
| | | | | $\Omega^* \leq \Omega_{limit}$ | $\Omega^* > \Omega_{limit}$ |
| Sector I | $V_8(000011000011)$ | $V_2(000000000011)$ | Sector VI → Sector I | $U_2(010011000011)$ | $U_8(110011000011)$ |
| Sector II | $V_9(001111000000)$ | $V_3(000011000000)$ | Sector I → Sector II | $U_3(001111000010)$ | $U_9(001111000011)$ |
| Sector III | $V_{10}(001100000011)$ | $V_4(001100000000)$ | Sector II → Sector III | $U_4(001101000011)$ | $U_{10}(001111001100)$ |
| Sector IV | $V_{11}(000000111100)$ | $V_5(000000001100)$ | Sector III → Sector IV | $U_5(001000111100)$ | $U_{11}(001100111100)$ |
| Sector V | $V_{12}(110000110000)$ | $V_6(000000110000)$ | Sector IV → Sector V | $U_6(110000110100)$ | $U_{12}(110000111100)$ |
| Sector VI | $V_7(110000000011)$ | $V_1(110000000000)$ | Sector V → Sector VI | $U_1(110000100011)$ | $U_7(110000110011)$ |



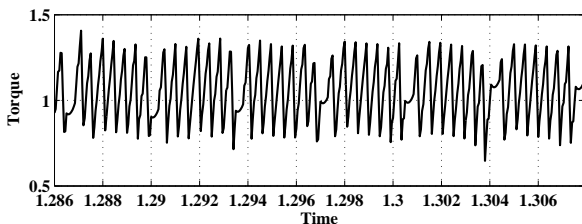
(a1)



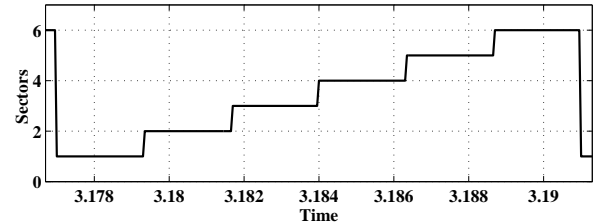
(b1)



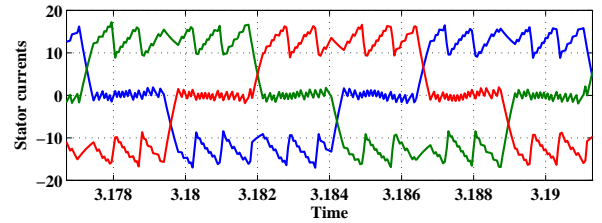
(c1)



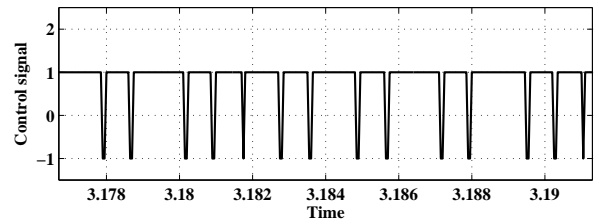
(d1)



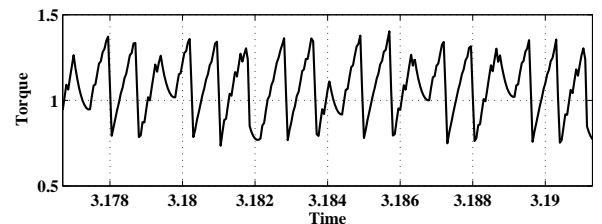
(a2)



(b2)



(c2)



(d2)

Figure 9: Simulated steady-state variables provided by the classic DTC-1 scheme at $\Omega = +100\text{rad/s}$ (subscript "1") and $\Omega = +150\text{rad/s}$ (subscript "2"). **Legend** (a): sector succession, (b): stator currents, (c): control signal c_τ and (d): electromagnetic torque.

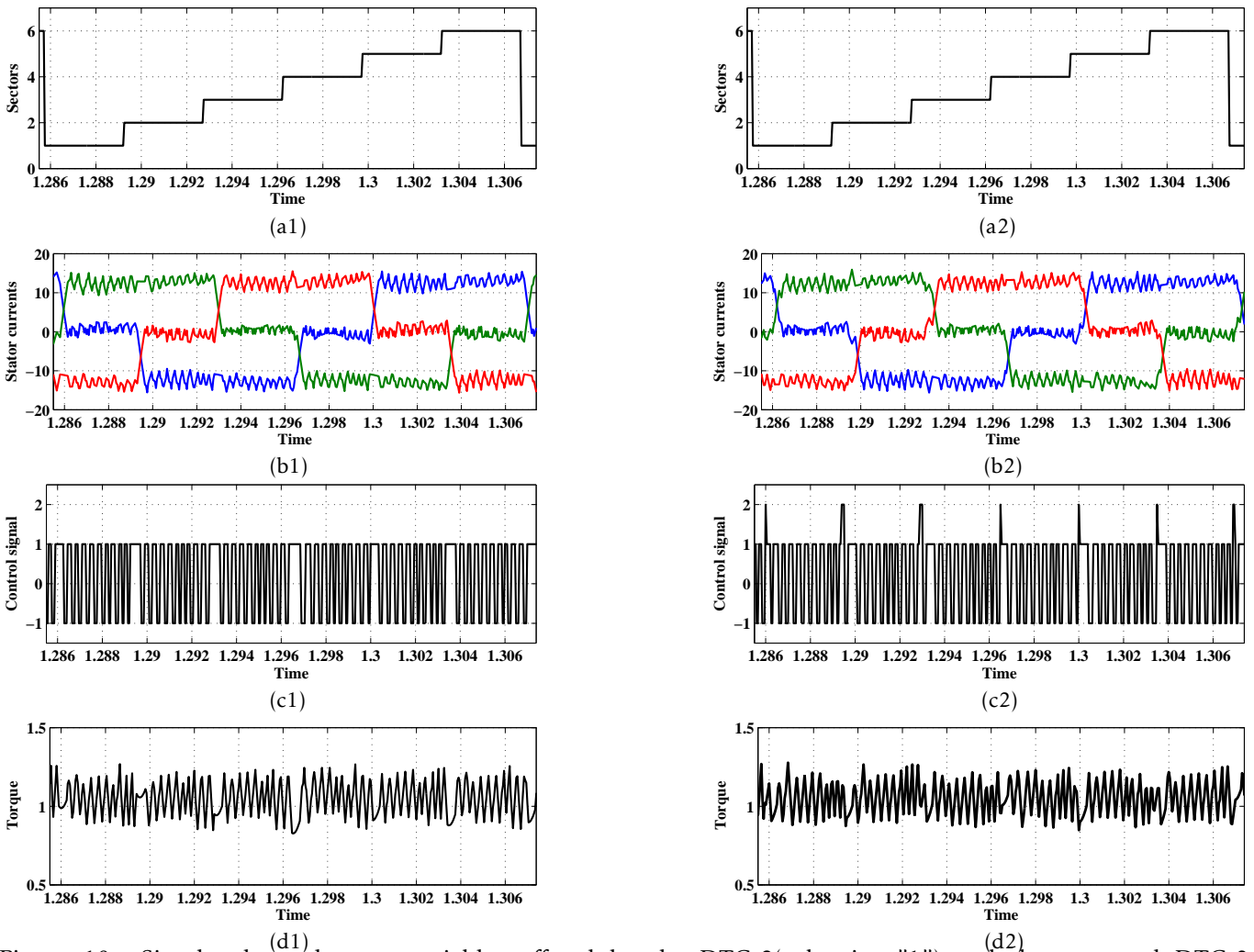


Figure 10: Simulated steady-state variables offered by the DTC-2(subscript "1") and the proposed DTC-3 (subscript "2") schemes at $\Omega = +100\text{rad/s}$. **Legend** (a): sector succession, (b): stator currents, (c): control signal c_τ and (d): electromagnetic torque.

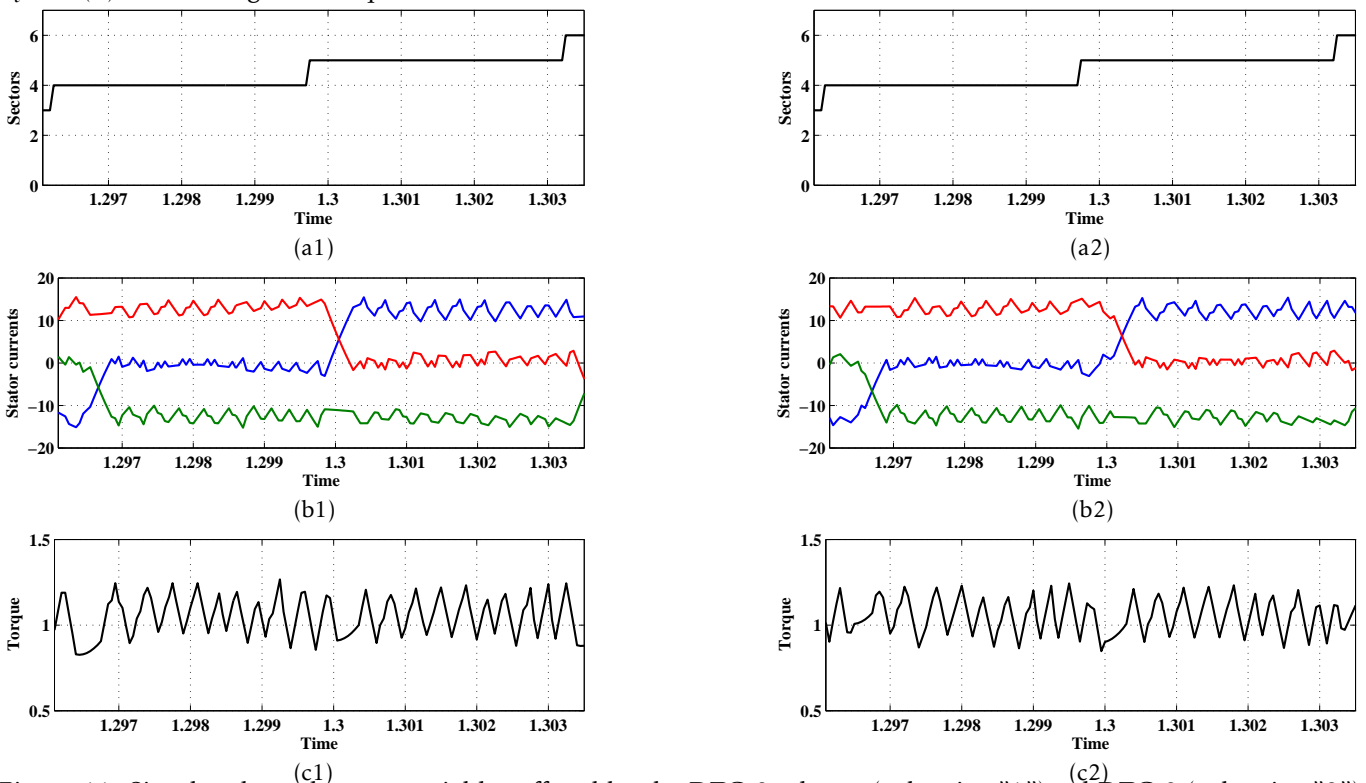


Figure 11: Simulated steady-state variables offered by the DTC-2 scheme (subscript "1") and DTC-3 (subscript "2") strategies for a speed $\Omega = +100\text{rad/s}$. **Legend** (a): commutation from sector IV to sector V, (b): the stator currents zoom, and (c): the electromagnetic torque zoom.

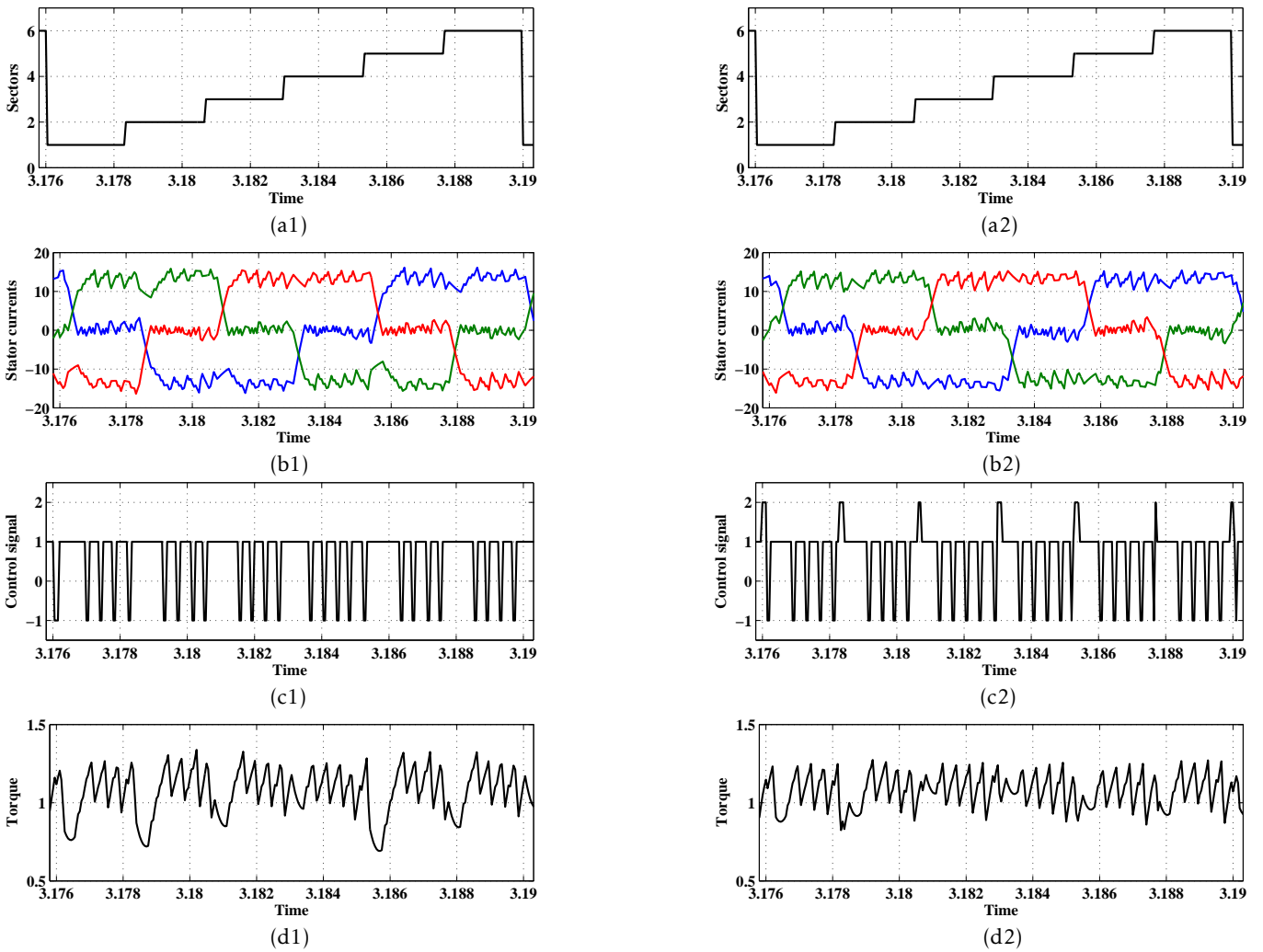


Figure 12: Simulated steady-state variables yielded by the DTC-2 (subscript "1") and the proposed DTC-3 strategies at $\Omega = +150\text{rad/s}$. **Legend** (a): sector succession, (b): stator currents, (c): control signal c_r and (d): electromagnetic torque.

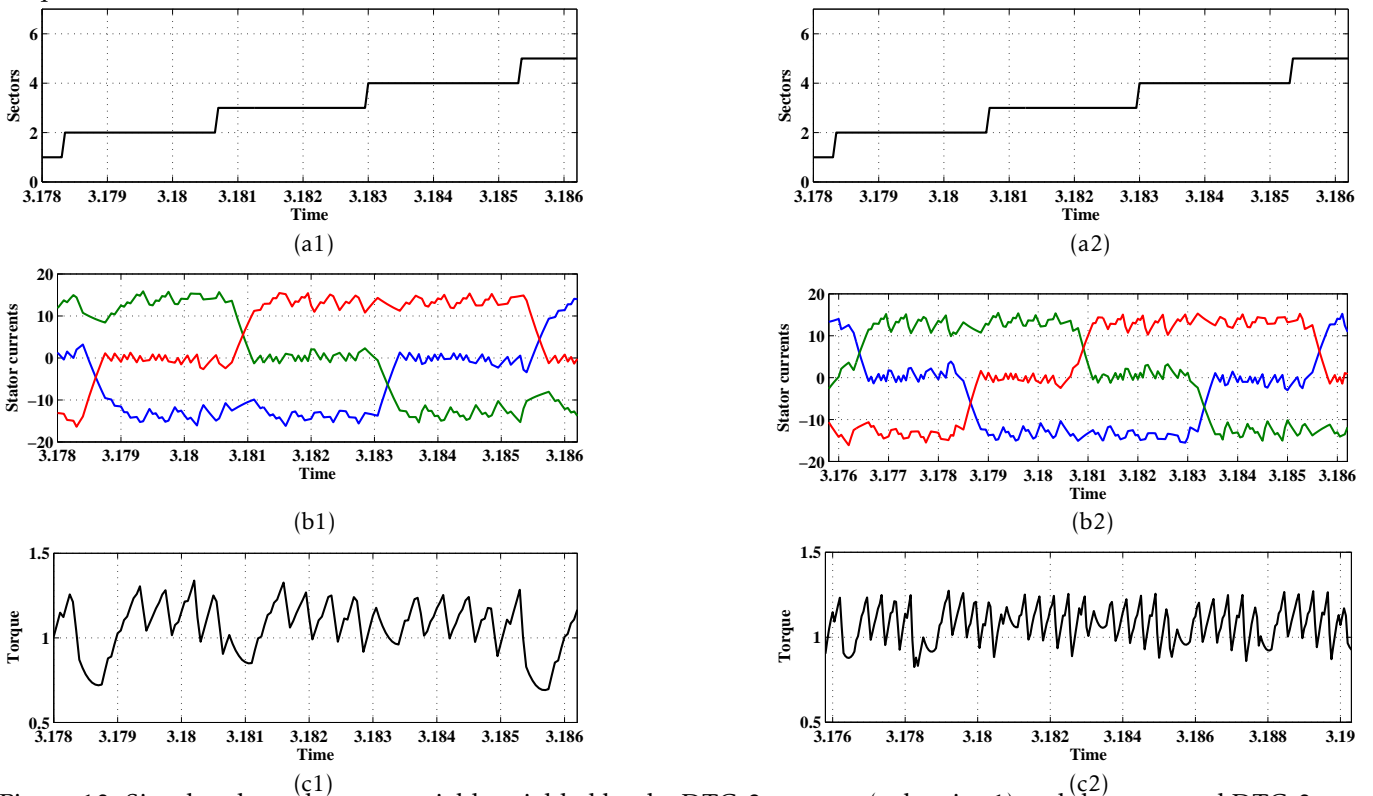


Figure 13: Simulated steady-state variables yielded by the DTC-2 strategy (subscript 1) and the proposed DTC-3 one for a speed $\Omega = +150\text{rad/s}$. **Legend** (a): commutations from sector II to sector IV, (b): the stator currents zoom, and (c): the electromagnetic torque zoom.

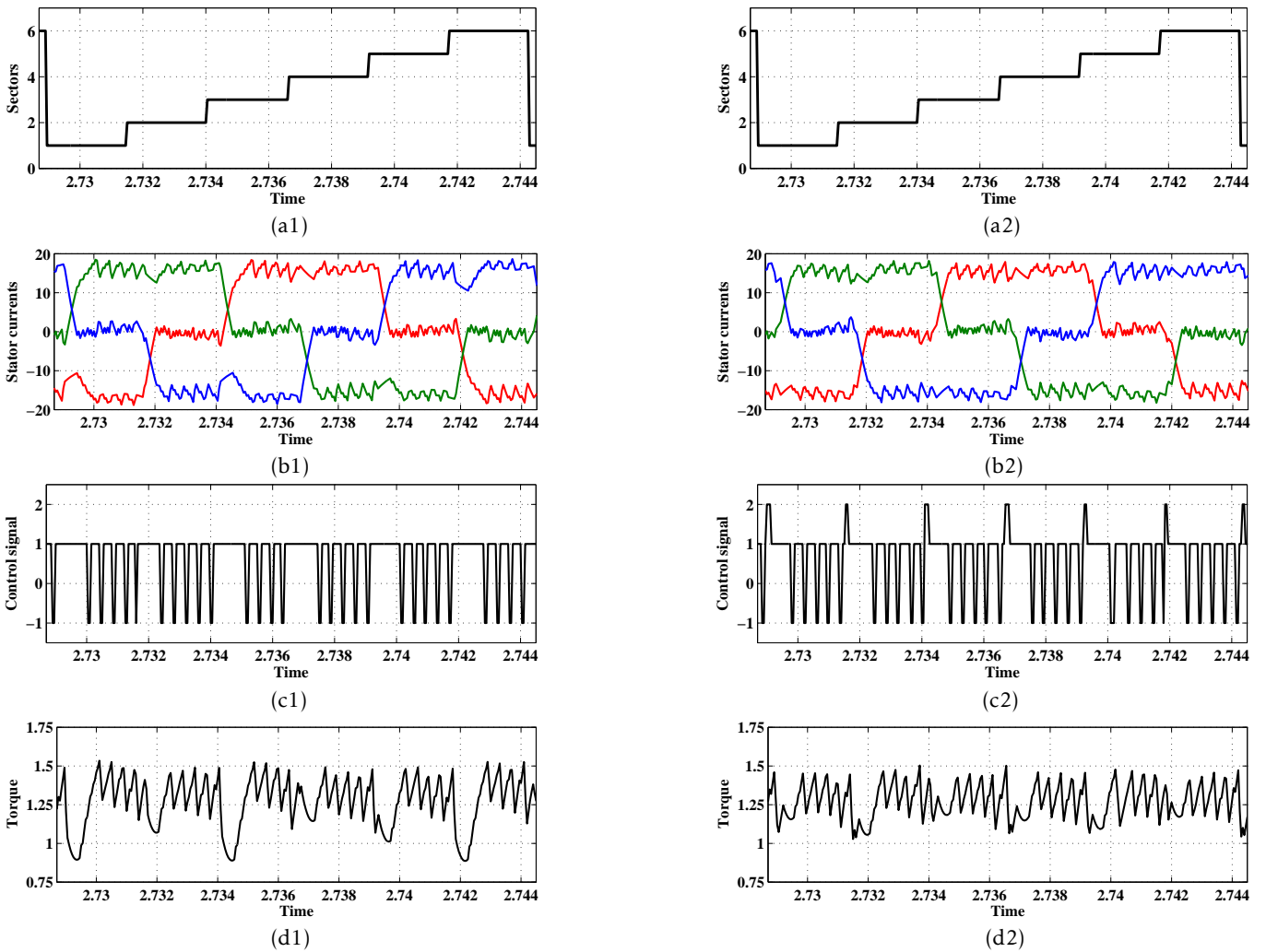


Figure 14: Simulated transient-state variables offered by the DTC-2(subscript "1") and the proposed DTC-3 schemes. **Legend** (a): sector succession, (b): stator currents, (c): control signal c_t and (d): electromagnetic torque.

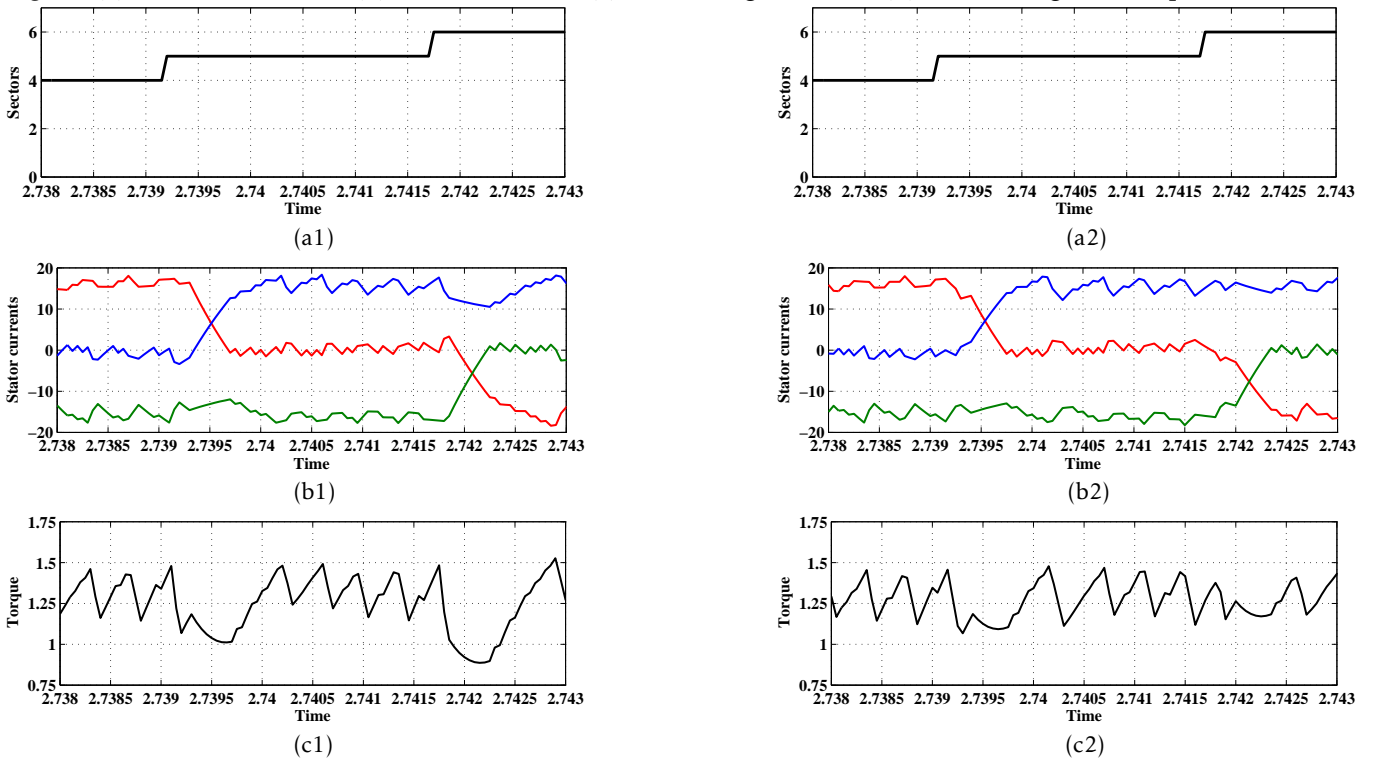


Figure 15: Simulated transient-state variables offered by the DTC-2 strategy (subscript 1) and the proposed DTC-3 one. **Legend** (a): commutations from sector V to sector VI, (b): the stator currents zoom, and (c): the electromagnetic torque zoom.

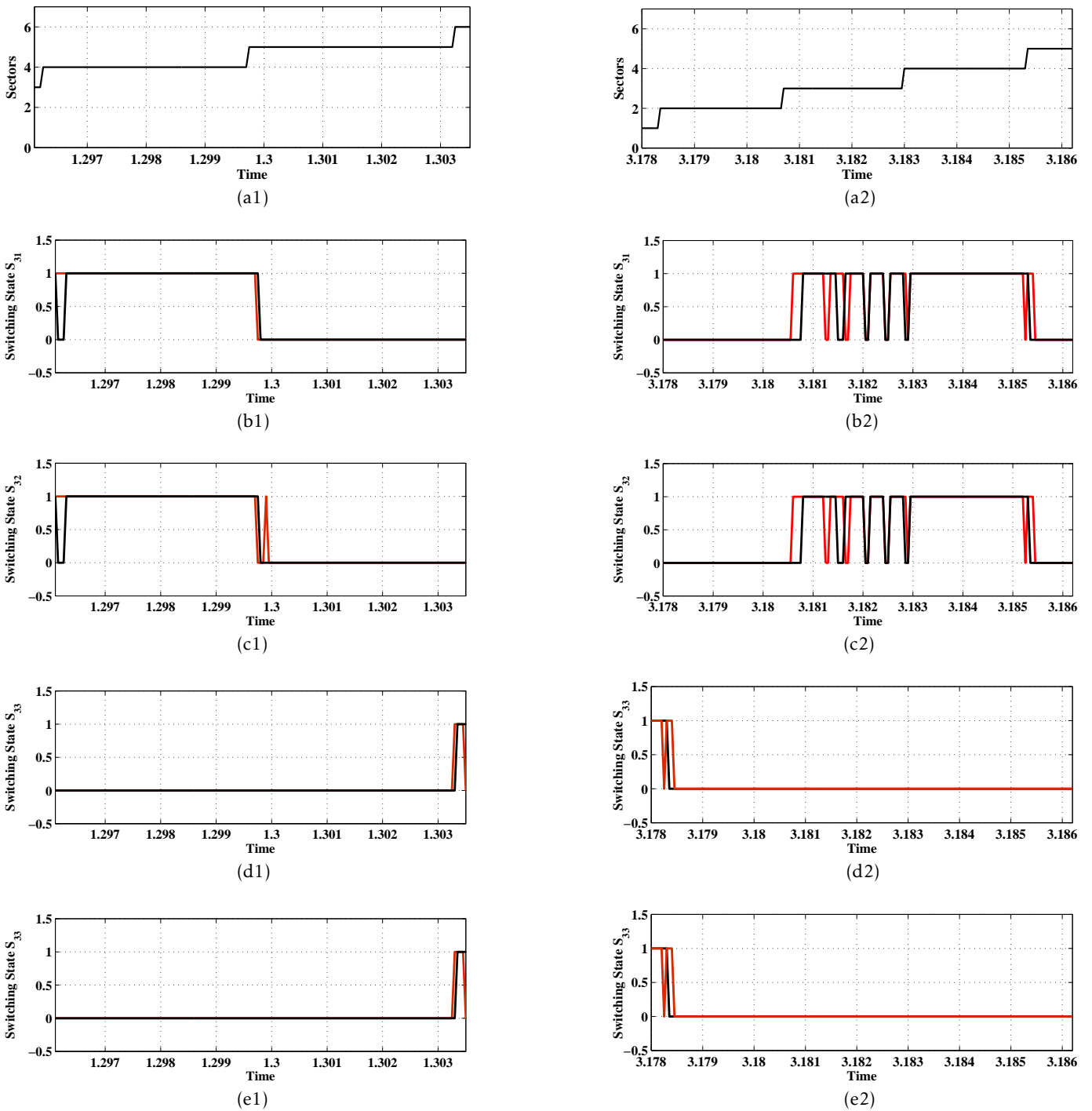


Figure 16: Simulated steady-state variables under the DTC-2 scheme (color black) and the proposed DTC-3 one (color red) for two reference speeds $\Omega = + 100\text{rad/s}$ (subscript 1) and $\Omega = + 150\text{rad/s}$ (subscript 2). **Legend** (a): commutations from sector II to sector IV, (b): S_{31} , (c): S_{32} , (d): S_{33} , and (e): S_{34} .

Moreover, simulation conditions characterizing the simulation study are listed below:

- a sampling period $T_s=55\mu s$,
- a proportional gain $K_p = 1$,
- an integral gain $K_i = 0.5$,
- a load torque = 1Nm,
- a limit speed $\Omega_{limit} = 110rad/s$
- the hysteresis bounds are: $\varepsilon_{\tau 1} = \pm 0.0012Nm$ and $\varepsilon_{\tau 2} = \pm 0.0036$.

To analyze the effectiveness of the proposed DTC-2 and DTC-3 strategies, this section deals with a simulation-based comparison between these strategies. By using MATLAB/SIMULINK, the proposed strategies are implemented. The obtained simulations results are illustrated in Figures. 10, 11, 12, 13, 14, 15.

4.1 Performance of the proposed strategies during sequence operation:

Figures.9, 10 and 12 show the waveforms of the current, the torque controller output c_τ and the torque waveforms at steady-state operation.

By comparing Figures.9(d), 10(d) and 12(d), one clearly notice that the DTC-1 scheme leads to an important torque dips thanks to the application of the Intermediate active voltage vectors. Both DTC-3 and DTC-2 strategies lead to a low torque dips during sequence operation thanks to the application of the Half active voltage vectors.

During sequence operation, both DTC-2 and DTC-3 schemes present almost the same torque waveforms. This is expected thanks to the application of the the same vectors. The difference concerns the torque decrease during commutations from sector to sector .

4.2 Performance of the proposed strategies during commutations from sector-to-sector :

To evaluate the proposed DTC schemes effectiveness during commutations from sector-to-sector , Figures. 11 and 13 give a zoom of the electromagnetic torque and the stator currents at steady-state operation. Figure.16 illustrates the steady-state waveforms of the switching states S_{31} , S_{32} , S_{33} and S_{34} with the sector succession.

As shown in Figures. 11(b1) and 13(b1), during the commutation from sector IV to sector V, the unbalancing between the current rising time and the current falling time affected the electromagnetic torque waveform. As a result of this, the DTC-2 strategy is penalized by a high torque dips. The comparison of Figures.10(c1) and 12(c1) confirms that commutation torque dips is more serious and more strong at high speed.

Compared to DTC-2, this commutation phenomenon is resolved for the DTC-3 strategy. Therefore, during the commutation from sector IV to sector V and in the case of the reference speed $\Omega^* = 150rad/s$ ($\Omega^* > \Omega_{limit}$), the current i_c is forced to flow through the IGBTs (S_{31} , S_{32}) and the supply source V_{dc} instead of the freewheeling diodes (D_{33} and D_{34}) as shown in Figures.16(b1), (b2), (b3) and (b4). However, from the analysis of Figures.16(a1), (a2), (a3) and (a4) in the case of a reference speed $\Omega^* = 100rad/s$ ($\Omega^* \leq \Omega_{limit}$), it can be clearly noticed that the current i_c is forced to flow through the IGBT S_{32} , the clamped diode and the supply source $\frac{V_{dc}}{2}$ instead of the freewheeling diodes (D_{33} and D_{34}). Consequently, $|di_c/dt|$ and $|di_a/dt|$ are equal for both reference speeds which results a high dynamic of the torque without commutation ripple. These benefits are confirmed in Figures. 11(a2), 11(a3), 13(b2) and 13(b3).

The performance of DTC strategies under a transient-state is presented in Figures.14 and 15. Accordingly, compared to DTC-2 and DTC-1 schemes, one can evidently affirm that the developed DTC-3 scheme leads to the lower commutation torque dips for both transient and steady-state operations.

5 Conclusion

BLDC motor is integrated in various applications due to its different advantages. However, the BLDC motor drive has the drawback of high torque ripple which affects the performance of this system. Thus, torque ripple minimization is a crucial necessity. This paper has been focused on the development of two DTC schemes dedicated to BLDC motor drives. Simulation work has been accomplished to highlight the developed schemes effectiveness and performances. It has been found that the developed DTC-3 scheme has guaranteed the less distortion in the line currents and less commutation torque dips. This developed strategy has been based on the compensation of the difference between the slopes of the incoming and outgoing phases currents.

References

- [1] J. Rodriguez, J.-S. Lai, and F. Z. Peng, "Multilevel inverters: A survey of topologies controls and applications", *IEEE Trans. Ind. Electron.*, vol. 49, no. 4, pp. 724-738, Aug. 2002.
- [2] Y. Liu, A. Q. Huang, W. Song, S. Bhattacharya, and G. Tan, "Smallsignal model-based control strategy for balancing individual dc capacitor voltages in cascade multilevel inverter-based statcom, *Industrial Electronics*", *IEEE Transactions on*, vol. 56, no. 6, pp. 2259-2269, 2009
- [3] H. Vahedi, K. Al-Haddad, P.-A. Labbe, and S. Rahmani, "Cascaded multilevel inverter with multicarrier pwm technique and voltage balancing feature", in *Industrial Electronics (ISIE)*, 2014 IEEE 23rd International Symposium on. IEEE, 2014, pp. 2155-2160
- [4] J. P. Lyons, V. Vlatkovic, P. M. Espelange, A. A. M. Esser, and F. F. Want, "Five level high power motor drive converter and control system", *U.S. Patent 6 058 031*, May 2, 2000.

- [5] S. Bernet, T. Bruckner, and P. Stiemer, Three-point converter and method for its operation, U.S. Patent 6 219 265, Apr. 17, 2001.
- [6] M. A. Doss, E. Premkumar, G. R. Kumar, and J. Hus-sain, "Harmonics and torque ripple reduction of Brushless DC Motor (BLDCM) using cascaded H-bridge multilevel in-verter", in *Proc. IEEE ICPEC*, Feb. 2013, pp. 296299.
- [7] Chan, C. C., Jiang, J. Z., Xia, W., Chan, K. T. "Novel wide range speed control of permanent magnet brushless motor drives". *IEEE transactions on power electronics*, 10(5), 539-546,1995
- [8] T. Shi, Y. Guo, P. Song, and C. Xia, "A new approach of minimizing commutation torque ripple for brushless DC motor based on DC-DC converter", *IEEE Trans. Ind. Electron.*, vol. 57, no. 10, pp. 3483-3490, Oct. 2010.
- [9] K. Ohishi, M. Nakao, K. Ohnishi, and K. Miyachi, "Microprocessor-controlled DC motor for load-insensitive position servo system", *IEEE Trans. Ind. Electron.*, vol. 34, no. 1, pp. 44-49, 1987.
- [10] X. Huang, A. Goodman, C. Gerada, Y. Fang, and Q. Lu, "A single sided matrix converter drive for a brushless dc motor in aerospace applications", *IEEE Trans. Ind. Electron.*, vol. 59, no. 9, pp. 3542-3552, Sep. 2012.
- [11] T. M. Jahns and W. I. Soong, "Pulsating torque minimiza-tion techniques for permanent magnet AC motor drives-a re-view", *IEEE Trans. Ind. Electron.*, vol. 43, no. 2, pp. 321-330, Apr. 1996.
- [12] X. Li, C. Xia, Y. Cao, W. Chen, and T. Shi, "Commuta-tion torque ripple reduction strategy of Z-source inverter fed brushless DC motor", *IEEE Trans. Power Electron.*, vol. 31, no. 11, pp. 7677-7690, Nov. 2016.
- [13] C. Xia, Y. Xiao, W. Chen, and T. Shi, "Torque ripple reduction in brushless DC drives based on reference current optimiza-tion using integral variable structure control", *IEEE Trans. Ind. Electron.*, vol. 61, no. 2, pp. 738-752, Feb. 2014.
- [14] G. Buja, M. Bertoluzzo, and R. K. Keshri, "Torque ripple-free operation of PM BLDC drives with petal-wave current sup-ply", *IEEE Trans. Ind. Electron.*, vol. 62, no. 7, pp. 4034-4043, Jul. 2015.
- [15] J. Fang, H. Li, and B. Han. "Torque ripple reduction in BLDC torque motor with non-ideal back EMF", *IEEE Trans. Power Electron.*, vol. 27, no. 11, pp. 4630-4637, Nov. 2012.
- [16] W. Jiang, Y. Liao, J. Wang, P. Wang, and Y. Xie, "Improved control of BLDCM considering commutation torque ripple and commutation time in full speed range", *IEEE Trans. Power Electron.*, vol. 33, no. 5, pp. 4249-4260, June 2018.
- [17] I. Takahashi and T. Noguchi, "A new quick-response and high efficiency control strategy of an induction motor", *IEEE Trans. Ind. Appl.*, vol. 22, no. 5, pp. 820-827, 1986.